

Feasibility of Logical Bell State Generation in Memory Assisted Quantum Networks

Vladlen Galetsky
TUM, Germany
vladlen.galetsky@tum.de

Nilesh Vyas
Airbus Central R&T, Germany
nilesh.vyas@airbus.com

Alberto Comin
Airbus Central R&T, Germany
alberto.comin@airbus.com

Janis Nötzel
TUM, Germany
janis.noetzel@tum.de

Abstract—This study explores the feasibility of utilizing quantum error correction (QEC) to generate and store logical Bell states in heralded quantum entanglement protocols, crucial for quantum repeater networks. Two novel lattice surgery-based protocols (local and non-local) are introduced to establish logical Bell states between distant nodes using an intermediary node. In the local protocol, the intermediary node creates and directly transmits the logical Bell states to quantum memories. In contrast, the non-local protocol distributes auxiliary Bell states, merging boundaries between pre-existing codes in the quantum memories.

We simulate the protocols using realistic experimental parameters, including cavity-enhanced atomic frequency comb quantum memories and multimode fiber-optic noisy channels. The study evaluates rotated and planar surface codes alongside Bacon-Shor codes for small code distances ($d = 3, 5$) under standard and realistic noise models. We observe pseudo-thresholds, indicating that when physical error rates exceed approximately $p_{\text{err}} \sim 10^{-3}$, QEC codes do not provide any benefit over using unencoded Bell states. Moreover, to achieve an advantage over unencoded Bell states for a distance of 1 km between the end node and the intermediary, gate error rates must be reduced by an order of magnitude ($0.1p_{\text{err}_H}$, $0.1p_{\text{err}_{CX}}$, and $0.1p_{\text{err}_M}$), highlighting the need for significant hardware improvements to implement logical Bell state protocols with quantum memories. Finally, both protocols were analyzed for their achieved rates, with the non-local protocol showing higher rates, ranging from 6.64 kHz to 1.91 kHz, over distances of 1 to 9 km between the end node and the intermediary node.

Index Terms—Quantum repeaters, quantum networks, lattice surgery, logical Bell pairs, logical heralded entanglement protocol, Bacon-Shor codes, surface codes.

I. INTRODUCTION

The vision for a quantum internet, as outlined in [1], is fundamentally rooted in fault-tolerant quantum communication. This requires the integration of quantum repeaters equipped with highly efficient and robust quantum memories for terrestrial links, and free-space quantum links facilitated by satellite-ground communication. Quantum repeater architectures have been meticulously designed [2], [3] to address errors primarily arising from photon loss, where photons are either absorbed or scattered and gate operation errors, which result from device imperfections causing noise and reduced fidelity.

Logical Bell pair generation is a fundamental building block for quantum repeater networks, ensuring high fidelity and reliable entanglement distribution during transmission and processing. Consequently, quantum repeater architectures are

classified into three generations, each introducing progressively advanced error correction methods [2], [3]. Quantum repeaters, utilizing probabilistic error suppression to manage practical imperfections [4], have seen significant progress in recent times. Milestone experiments have demonstrated heralded entanglement distribution between two absorptive quantum memories [5], [6], realization of a multimode quantum network of remote solid-state qubits [7], entanglement of trapped-ion qubits separated by 230 m [8]. However, these demonstrations are limited in achieving the high fidelity and long-distance communication essential for a scalable quantum internet [1], [3].

Incorporating quantum error correction (QEC) to mitigate errors signifies a major leap forward, promising more robust and scalable quantum networks. However, despite their immense potential, there has been relatively limited research on the implementation of QEC for generating and storing logical Bell pairs in a quantum network scenario, compared to the extensive experimental efforts on heralded entanglement generation. This highlights the critical need for a comprehensive feasibility study on the generation of logical Bell pairs and their storage in quantum memories.

This work endeavors to bridge the existing research gap by conducting detailed simulations on generating logical Bell pairs using lattice surgery within a noise and error model that incorporates experimental parameters. We design two new memory-dependent logical heralded entanglement protocols relying on a local and non-local logical Bell pair generation, respectively and we study their performance while evaluating the practical challenges associated with various QEC codes. We aim to gain vital insights into their viability and identify key experimental parameters requiring further development.

II. OUR CONTRIBUTIONS

This study expands upon the latest developments in heralded quantum entanglement generation, a building block of any quantum repeater protocol. By utilizing QEC codes in quantum memories, we correct logical Bell states in a fault-tolerant manner. We analyze the feasibility, challenges, and benefits of generating and storing these states through detailed simulations incorporating realistic experimental parameters. This work is the first to analyze the feasibility of non-local logical Bell states in quantum networks, with quantum error correction (QEC) performed in a quantum memory.

arXiv:2412.01434v2 [quant-ph] 3 Dec 2024

We propose a configuration where Alice and Bob, two distant nodes, aim to establish a logical Bell pair with the help of an intermediary node, Charlie. This work introduces two new protocols for executing the heralded entanglement protocol with logical Bell pairs: a local and a non-local scheme. Both protocols use heralding techniques to address loss errors and employ quantum error correction via lattice surgery to construct and correct a logical Bell state. In the local protocol, Charlie performs lattice surgery to generate the logical Bell state locally and directly transmits it to Alice and Bob, storing the Bell states in quantum memory for later measurement. In the non-local protocol, Charlie distributes physical entanglement pairs to Alice and Bob, who independently perform lattice surgery during d merging cycles to generate a logical Bell state in a distributed manner.

Our simulations incorporate a cavity-enhanced atomic frequency comb quantum memory and a multimode fibre-optic noisy channel, accounting for various experimental variables (Table I). We evaluate the feasibility of generating and storing logical Bell states using $d = 3$ and $d = 5$ surface and Bacon-Shor codes within this comprehensive noise simulation framework.

Considering the standard noise model described in Section V-A, we identify pseudo-thresholds where physical error rates exceeding physical error rates above $p_{\text{err}} = (5.5 \pm 0.2) \times 10^{-4}$ for $S[[18, 2, 3]]$, $p_{\text{err}} = (9.0 \pm 0.3) \times 10^{-4}$ for rotated $S[[18, 2, 3]]$, and $p_{\text{err}} = (1.5 \pm 0.2) \times 10^{-3}$ for the $BS[[18, 2, 3]]$ codes provide no advantage over unencoded Bell states in either protocol. These findings extend the results of [9], which reported pseudo-thresholds of $p_{\text{err}} = 9.0 \times 10^{-3}$ for Bacon-Shor codes and $p_{\text{err}} = 1.5 \times 10^{-3}$ for surface codes, both assessed without lattice surgery and idle qubit consideration.

We also determined the thresholds at which increasing the code distance worsens the logical error rate [10] (p_L). By comparing $S[[18, 2, 3]]$ with $S[[50, 2, 5]]$, we found thresholds of $p_{\text{err}} = (3.9 \pm 0.1) \times 10^{-3}$ for BS codes and $p_{\text{err}} = (5.8 \pm 0.2) \times 10^{-3}$ for rotated S codes.

Using a more realistic noise model, as described in Section V-B, we reevaluated these thresholds in terms of gate error rates p_{err_H} , $p_{\text{err}_{CX}}$, and p_{err_M} , with parameters provided in Table I. For a node-to-Charlie distance of $D = 1$ km, achieving an advantage over an unencoded Bell state heralded protocol requires reducing gate error rates by an order of magnitude ($0.1p_{\text{err}_H}$, $0.1p_{\text{err}_{CX}}$, and $0.1p_{\text{err}_M}$). This result offers critical insight into the hardware improvements necessary to implement logical Bell state protocols with quantum memories.

In the same noisy environment, we found a threshold of 0.58 ± 0.01 for rotated S codes, determined by the ratio of gate errors to the logical error rate. However, due to the gate complexity of implementing multi-Pauli product operators on IBM processors, as described in Appendix X-B, the threshold for BS codes degrades by two orders of magnitude compared to surface codes.

To assess the feasibility of the protocol, we evaluated the protocol rate, where the second protocol (non-local) demonstrated a clear advantage in success rate R_{success} . For

$S[[18, 2, 3]]$, the success rate ranged from $R_{\text{success}} \in [6.64 \pm 0.12, 3.22 \pm 0.04]$ kHz, while for $BS[[18, 2, 3]]$, it ranged from $R_{\text{success}} \in [2.74 \pm 0.05, 1.91 \pm 0.03]$ kHz, across distances of 1 km to 9 km between the nodes and Charlie. This advantage is attributed to two key factors: the stringent requirement of protocol 1 (local) to abort if any data qubits are lost during transport or storage, and the higher source frequency (f_{source}) for auxiliary Bell pair generation in node-merging operations in protocol 2.

Having defined the hardware requirements for logical Bell state memory-assisted protocols, we explore future prospects and challenges associated with utilizing quantum error correction in quantum memories.

III. PRELIMINARIES

A. Notation

This paper uses Dirac notation for quantum states and capital letters for quantum gates. General quantum error correction (QEC) codes are denoted as $C[[n, k, d]]$, where n is the number of data qubits, k is the number of logical qubits, d is the code distance and C is the initial of the name of the code. Specific codes are represented as $S[[n, k, d]]$ for surface codes, $BB[[n, k, d]]$ for bivariate bicycle codes, and $BS[[n, k, d]]$ for Bacon-Shor codes, providing a consistent framework for describing codes, subcodes, and low-density parity-check (LDPC) codes.

We introduce the unitary operators X (Pauli- X) and Z (Pauli- Z) by describing their action on the computational basis of $\mathcal{H} = \mathbb{C}^2$: $X|j\rangle = |j \oplus 1\rangle$ and $Z|j\rangle = (-1)^j|j\rangle$. Similarly, we define the Hadamard gate H and the CNOT gate CX as:

$$H|j\rangle = \frac{1}{\sqrt{2}}(|0\rangle + (-1)^j|1\rangle), \quad (1)$$

$$CX|i, j\rangle = |i, i \oplus j\rangle, \quad (2)$$

where i and $j \in \{0, 1\}$. In summary, all quantum circuits adhere to the standard quantum computation formalism: time progresses from left to right and measurements for the QEC code are performed on a computational basis.

B. Glossary

For a general quantum error correction code $C[[n, k, d]]$ we introduce a new concept of code separability:

Definition 1. *Code separability: A code $C[[n, k, d]]$ is separable if it can be split into two independent codes: $C[[n, k, d]] \rightarrow (C_1[[n-s, k-a, d]], C_2[[s, a, d]])$, without compromising the original code's architecture or distance d . Where, code $C_1[[n-s, k-a, d]]$ consists of $n-s$ data and $k-a$ logical qubits, and $C_2[[s, a, d]]$ consists of s data and a logical qubits.*

An example of a separable code can be viewed in [11] for the split operation using lattice surgery in surface codes (S): $S[[27, 3, 3]] \rightarrow (S_1[[18, 2, 3]], S_2[[9, 1, 3]])$. A generalization of such is presented in the context of Calderbank-Shor-Steane (CSS) code surgery [12].

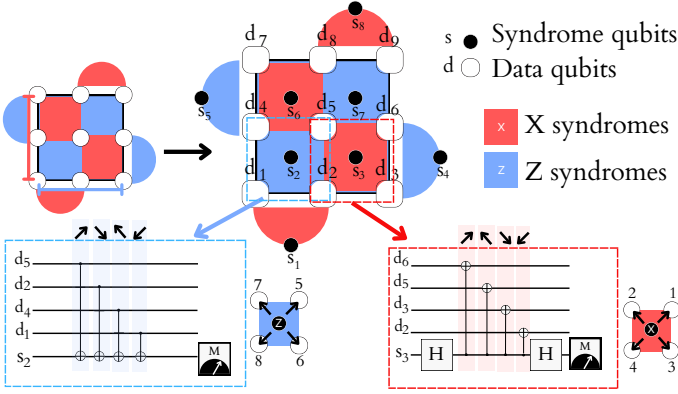


Fig. 1. Example of $d = 3$ rotated surface code, with respective Z and X syndrome measurements. The set of X -stabilizers is associated with red plaquettes, while Z -stabilizers correspond to blue plaquettes. Since neighboring plaquettes always share two vertices, the stabilizers commute for any arrangement of plaquettes. The order of operations is presented with arrows between the X/Z syndrome qubits and data qubits.

We also define the concepts of threshold and pseudo-thresholds error rate of a code family and code, according to [13]:

Definition 2. *Threshold error rate:* For a given noise model and code family, the threshold is the maximum physical error rate at which increasing the code distance (as $d \rightarrow \infty$) no longer results in an improvement in the logical error rate.

Definition 3. *Pseudo-threshold error rate:* For a given noise model, the pseudo-threshold is the maximum physical error rate at which a specific code $C[[n, k, d]]$ achieves the same logical error rate as the unencoded case.

This work uses pseudo-threshold to compare the performance of unencoded Bell states with their logical counterparts.

C. Choice of QEC Codes

We focus on the subsystem CSS Bacon-Shor code $BS[[9, 1, 3]]$ and the CSS surface code $S[[9, 1, 3]]$, both of which are well-suited for current hardware, enabling QEC with smaller circuit sizes and reducing noise errors. More specifically for S codes, we consider both the planar lattice and a rotated one as described in [11]. An example of rotated S code for $d = 3$ is demonstrated in Fig. 1. We also consider in this work $BS[[25, 1, 5]]$ and $S[[25, 1, 5]]$ codes, however, they are only used to calculate the code thresholds as their implementation in the noise model described in Section V-B is currently unfeasible due to the high qubit noise and loss. For a more indepth view of Surface codes and Bacon-shor codes operation see Appendix. X-A.

While bivariate bicycle codes (BB) are more scalable, their smallest configuration $BB[[18, 4, 4]]$ and $BB[[18, 2, 2]]$ are not directly separable and hence not comparable with $S[[9, 1, 3]]$ or $BS[[9, 1, 3]]$ codes. Meaning we would need to generate a $BB[[36, 8, 4]]$ or $BB[[36, 4, 2]]$ code to encode a logical Bell pair, the added logical qubits could be used to enhance

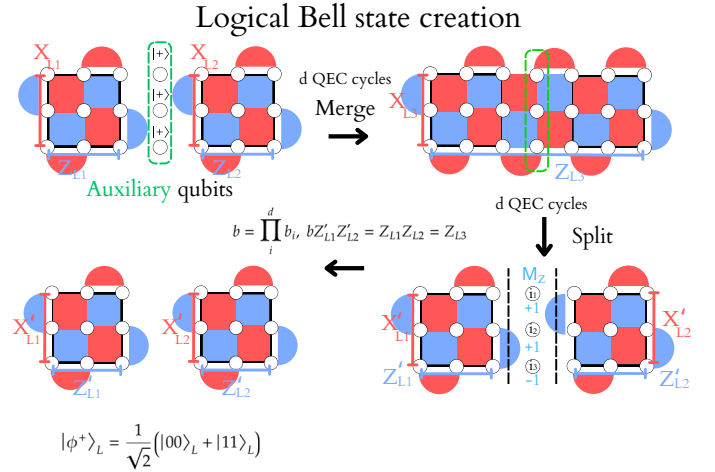


Fig. 2. Lattice surgery for creating logical Bell states by merging and splitting operations on a rotated surface code.

redundancy or support logical Bell pair distillation [14], [15]. Additionally, the choice of quantum error correction codes must align with the physical constraints of the protocol. While toric codes [16] and BB codes [17] offer potential benefits, their operations must be compensated in hardware due to repeated boundary conditions.

We also considered utilizing hybrid surface and Bacon-Shor codes, as discussed in [18]. These codes are tailored to the IBM processor architecture (with the noise model applied in our analysis) and, for $d = 3$, yield the hybrid $S|BS[[18, 2, 3]]$ code. Despite the code's strong adaptability to the IBM processor architecture, its non-separability renders it incomparable to the $d = 3$ S and BS codes individually.

D. Lattice surgery

Lattice surgery is a technique that enables the splitting and merging of patches, thereby facilitating universal logical operations [11], [19]. Each operation incurs a time cost proportional to the code distance d , with one unit of time approximately equating d [19]. Single logical qubit initializations can be achieved with states $|+\rangle$, $|-\rangle$, $|0\rangle$ and $|1\rangle$ through transversal initialization, and states $|i\rangle$ and $|-i\rangle$ via topological initialization using twists. Arbitrary states can be approximated using Clifford + T gate circuits [20], with no additional time cost for single qubit logical initializations.

Entanglement-based initialization requires the merging and splitting of patches, adding an extra time cost of d cycles. An example of logical Bell state generation is presented in Fig. 2 for an X boundary in a rotated $S[[18, 2, 3]]$ code.

A more in-depth explanation can be found in [11], [21], [22] but in summary d auxiliary data qubits are initialized in the basis of the lattice surgery either $|0\rangle$ or $|+\rangle$, during d QEC cycles the merging operation occurs. The merge operation realizes a $X_{L1} \otimes X_{L2}$ measurement, joining the boundaries between two codes.

Later on the split operation occurs, measuring the auxiliary qubits, the logical operations of the splitted codes X'_{L1} and X'_{L2} both commute the split operation. Z_{L3} decomposes as $Z_{L3} = Z_{L1}Z_{L2} = bZ'_{L1}Z'_{L2}$ with an added correction b as seen in Fig. 2, defined by the sign of the product of the measurements b_i of the auxiliary qubits. After the codes are split and the correction is performed the logical Bell pairs are generated $|\phi^+\rangle_L = \frac{1}{\sqrt{2}}(|00\rangle_L + |11\rangle_L)$.

Lattice surgery for Bacon-Shor codes is performed in a similar manner, the strategy used is outlined in [23].

Entanglement-based QEC is relatively new, Erhard et al. (2021) [24] demonstrated experimentally local logical quantum teleportation using lattice surgery with two $d = 2$ surface codes on an ion trap quantum processor, suggesting its viability in a quantum network scenario if studied non-locally.

IV. LOGICAL BELL PAIR PROTOCOLS

We propose two new protocols as seen in Fig. 3, a local (left) and a non-local (right) logical heralded entanglement, both of which leverage QEC and lattice surgery techniques in a multi-mode quantum storage to ensure robustness against quantum noise and operational errors.

A. Local logical Bell pair protocol

The local protocol involves generating logical Bell pairs locally by Charlie, taking advantage of the physical proximity of qubits to perform error correction and lattice surgery operations efficiently. Locally generated logical qubits are then shared with Alice and Bob over a quantum channel. This method typically involves splitting and merging logical qubits to create entangled states, with QEC codes ensuring that the logical qubits remain fault-tolerant throughout the process.

Protocol 1 Local logical Bell pair protocol

- 1) Charlie constructs two QEC codes $C[[n, k, d]]$.
 - 2) Using lattice surgery, Charlie merges each pair of codes and waits for d QEC cycles.
 - 3) Charlie then splits the merged codes, and then transmits n data qubits to Alice and Bob through a multi-modal quantum channel.
 - 4) The protocol only continues if all data qubits are successfully gathered and stored in quantum memory; otherwise, it is aborted.
 - 5) The logical qubits in the quantum memory undergo correction for m_1 cycles. Subsequently, the logical qubits k are measured, and the results are communicated between both parties via a classical channel.
-

B. Non-local logical Bell pair protocol

The non-local protocol focuses on generating logical Bell pairs between spatially separated Alice and Bob. This approach extends the principles of QEC and lattice surgery to a distributed environment, where the boundaries of the codes are extended non-locally during d merging cycles using auxiliary

Bell states. Non-local logical Bell pair generation requires advanced techniques to manage the additional challenges posed by noise and decoherence over long distances, but those challenges are heavily compensated by the high frequency of the auxiliary Bell state generation compared to the local scheme.

Protocol 2 Non-local logical Bell pair protocol

- 1) Both Alice and Bob possess a $C[[n, k, d]]$ code in their quantum memory.
 - 2) Charlie generates d auxiliary Bell-pairs during d lattice surgery merging cycles and sends them through a multimodal quantum channel to Alice and Bob.
 - 3) If for one of the d cycles, the auxiliary Bell pairs are lost, the protocol continues and a newly generated auxiliary Bell pair is sent.
 - 4) Alice and Bob expand the boundary of their respective codes using d auxiliary Bell pairs over d cycles of syndrome measurement. They merge the two codes via entanglement using lattice surgery.
 - 5) Alice and Bob then split the merged qubits, resulting in the creation of two maximally entangled codes.
 - 6) The logical qubits in the quantum memory are corrected over m_1 cycles. Subsequently, the logical qubits k are measured, and the results are shared between both parties via a classical channel.
-

C. Comparison of the two Protocols

Both protocols require d^2 data qubits to execute Bell pair production. Switching from protocol 1 to protocol 2 introduces a trade-off: the non-local scheme (protocol 2) reduces the need for multiplexing in the optical multi-mode channel for state transport, however at the same time, it increases the number of cycles (d cycles) required to utilize the multi-mode channel.

In a scenario where the bottleneck is the multiplexing capability of the quantum memory, which can store only one Bell state at a time, both protocols operate in two distinct regimes.

The first regime arises when the combined time for state generation (t_{gen}) and distribution (t_{travel}) from Charlie is shorter than or equal to the duration of the QEC cycles ($t_{\text{QEC}} = m_1 t_{\text{cycle}}$) in the memory, such that $t_{\text{gen}} + t_{\text{travel}} \leq t_{\text{QEC}}$.

The second regime arises when $t_{\text{gen}} + t_{\text{travel}} > t_{\text{QEC}}$, causing the logical Bell pairs generated by Charlie to remain idle until node hardware becomes available, due to occupancy constraints.

The main benefit of the protocol 1 is the early creation of fault-tolerant, maximally entangled logical pairs, reducing noise over d cycles. Conversely, the protocol 2 allows for resource-intensive entanglement purification at Alice's and Bob's nodes before encoding the Bell states, allowing even to perform purification for each of the d^2 auxiliary Bell pairs depending on environmental noise. For instance, achieving a

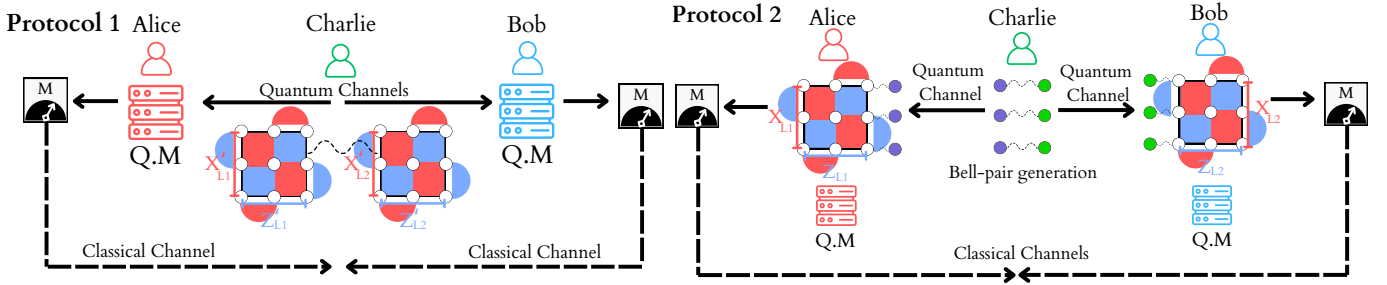


Fig. 3. Proposed protocols for QEC on a quantum memory for heralded entanglement protocol. Protocol 1 (left) and Protocol 2 (right) represent the local/non-local generation of logical Bell states, respectively. For Protocol 1 the data qubits are transmitted to Alice and Bob using a multi-mode channel and stored in a quantum memory (Q.M) while in protocol 2 auxiliary Bell pairs are generated entangling for d cycles the boundaries of the codes already present inside the quantum memories.

fideliy of $F = 0.99$ from $F = 0.85$ may require approximately $5d^2$ auxiliary Bell pairs, as extrapolated from the results in [25]. This estimation assumes no loss of Bell pairs during transportation or storage in the merging operation of protocol 2.

In protocol 1, the Bell pair generation time is limited by the logical Bell pair creation rate $f_{\text{gen}} = 1/t_{\text{merge}}$ with $t_{\text{gen}} = t_{\text{merge}}$. If a photon or data qubits are lost due to storage and recovery inefficiencies, faulty detection dark counts, or fiber loss, the protocol is aborted and restarted. In protocol 2, the auxiliary Bell pair generation frequency matches the source frequency, f_{source} . If any of the d Bell pairs fail during transportation or detection, we generate a new set of d Bell pairs for that merging cycle instead of restarting the entire protocol. If syndrome measurements fail to recover the data qubits, the protocol is aborted and restarted.

In protocol 2, the auxiliary Bell pairs act as data qubits for merging the boundaries of the two codes, at Alice's and Bob's ends, requiring d repetition cycles for each syndrome extraction step. Synchronization is vital between nodes, as protocol 2 depends on continuous classical communication to exchange syndrome measurements. However, this constraint is partially relaxed in protocol 1, where Charlie performs all lattice surgery operations prior to storing the states in quantum memory.

V. NOISE MODEL

A. Standard noise channel

The standard noise channel [9] is described by the following Kraus matrices for single-qubit and two-qubit channels:

$$K_1 = \left\{ \sqrt{1 - p_{\text{err}}} I, \sqrt{\frac{p_{\text{err}}}{3}} X, \sqrt{\frac{p_{\text{err}}}{3}} Y, \sqrt{\frac{p_{\text{err}}}{3}} Z \right\}, \quad (3)$$

$$K_2 = \left\{ \sqrt{1 - p_{\text{err}}} II, \sqrt{\frac{p_{\text{err}}}{15}} IX, \dots, \sqrt{\frac{p_{\text{err}}}{15}} ZZ \right\}. \quad (4)$$

In this model, the channel error probability is denoted as p_{err} . A noise channel is applied after each gate operation, and for measurement operations, the standard noise channel is applied beforehand. For idle qubits between operations, noise is modelled using the Kraus matrix K_1 , applied as

a channel with the same fixed p_{err} . This approach differs from the standard model in [9]. Additionally, this model does not account for decoherence and dephasing during the transportation and storage of quantum states.

For two-qubit parity measurements in the X and Z bases, denoted M_{XX} and M_{ZZ} , the measurement process includes both the measurement operation and a two-gate depolarization channel. This depolarization channel, characterized by the Kraus matrix K_2 , is applied to the qubits involved in the operation similarly to the method described in [23].

B. Robust noise channel

1) *Error model:* Gate and readout errors are based on calibration data from the IBM Sherbrooke 127-qubit quantum processor for each QEC cycle, as shown in Table I.

The *decoherence* and *dephasing* channel on a single qubit is described by the following transformation on a density matrix ρ [26]:

$$\rho \rightarrow \mathcal{E}_{\text{APD}}(\rho) = \begin{pmatrix} 1 - \rho_{11} e^{-\frac{t}{T_1}} & \rho_{01} e^{-\frac{t}{T_2}} \\ \rho_{01}^* e^{-\frac{t}{T_2}} & \rho_{11} e^{-\frac{t}{T_1}} \end{pmatrix}, \quad (5)$$

where t represents the execution or idle time of the gate, while T_1 and T_2 are the decoherence and dephasing times, respectively. The amplitude and damping channel can be approximated to an asymmetric depolarization channel (Pauli channel) using Pauli twirling [27], which removes the off-diagonal terms from Eq. 5 in the Pauli matrices representation, resulting in the following error probabilities [26], [28].

$$p_x = p_y = \frac{1 - e^{-\frac{t}{T_1}}}{4}, \quad p_z = \frac{1 - e^{-\frac{t}{T_2}}}{2} - \frac{1 - e^{-\frac{t}{T_1}}}{4}. \quad (6)$$

During logical Bell state transportation and each physical gate idle time in the quantum memory for each QEC cycle, these probabilities describe the damping channel. Using the same

TABLE I
SIMULATION PARAMETERS FOR THE ROBUST NOISE CHANNEL

Parameter	Value	Parameter	Value	Parameter	Value
Qubit decoherence time (T_1)	223.44 μs	Qubit dephasing time (T_2)	295.35 μs	Comb finesse (F)	40
Comb absorption efficiency (αl)	1.0	Reflectivity mirror 1 (R_1)	0.96	Reflectivity mirror 2 (R_2)	0.99
Comb FWHM linewidth (ϵ)	3 kHz	Photon indistinguishability	0.95	Source frequency (f_{source})	33 MHz
Detection efficiency (p_{detect})	0.95	Source wavelength	1550 nm	Fiber attenuation (τ)	0.17 dBkm $^{-1}$
Driven storage/recovery time	30 ns	Photon velocity in fiber	$2.08 \times 10^8 \text{ ms}^{-1}$	Dark count frequency (f_{dark})	10 Hz
CX gate ($p_{\text{err}_{\text{CX}}}$)	6.1×10^{-3}	H gate ($p_{\text{err}_{\text{H}}}$)	1.7×10^{-4}	Readout error ($p_{\text{err}_{\text{M}}}$)	7.7×10^{-3}
Mean CX gate time	533 ns	Mean H gate time	60 ns	Mean measurement time	1.216 μs

methodology for two-qubit gates, the following probability errors for all 16 combinations of X, Y, Z, I are obtained:

$$\begin{aligned}
p_{I(X/Y)} &= p_{(X/Y)I} = p_x(1 - p_x - p_y - p_z) \\
p_{(X/Y)(X/Y)} &= p_x p_x \\
p_{Z(X/Y)} &= p_{(X/Y)Z} = p_x p_z \\
p_{IZ} &= p_{ZI} = p_z(1 - p_x - p_y - p_z) \\
p_{ZZ} &= p_z p_z.
\end{aligned} \tag{7}$$

2) *Transmission channel*: For the transmission channel, we assume a multimode fiber optic channel sized to the data qubits. We use a source frequency of $f_{\text{source}} = 33 \text{ MHz}$ [29], with each photon sent through a multimode optical fiber channel. The source wavelength is chosen for compatibility with AFC quantum memories without additional frequency conversion losses, as demonstrated with erbium-doped crystal type AFC in [30]. The fiber loss channel is described by the single-photon transmission probability [31]

$$\eta_{\text{channel}} = 10^{-D\tau/10}, \tag{8}$$

with D being the transmission distance between the nodes (Alice and Bob) and Charlie, and $\tau = 0.17 \text{ dBkm}^{-1}$ being the fibre attenuation with a refractive index of glass in the fibre of $n_{\text{glass}} = 1.44$.

Before storage, the photon is detected from the fibre optical channel and we consider a detection efficiency of $p_{\text{detect}} = 0.9$ [29]. At the photon detector, we consider the dark count probability following the Poisson distribution [31]

$$\eta_{\text{dark}} = 1 - e^{-t_w f_{\text{dark}}}, \tag{9}$$

with a capture window of the detector being $t_w = 25 \text{ ns}$. f_{dark} is the frequency of dark counts, which has been experimentally determined to be approximately $f_{\text{dark}} \approx 10 \text{ Hz}$ [29].

3) *Quantum memory*: At both Alice's and Bob's locations, we employ multiple AFC-type memories [32], which couple directly with the photon's frequency, eliminating the need for additional conversions unlike Nitrogen vacancy centers or transmon coupled cavities. State-of-the-art single-mode AFC storage can achieve up to one hour of coherent storage time [33] using a zero first-order-Zeeman magnetic field and dynamical decoupling to protect spin coherence, achieving a fidelity of 96.4% [32], [34]. Multimode AFC memories have demonstrated capabilities of over 15 spatial \times 30 temporal modes [35] and 1060 temporal modes [36], with lifetimes

reaching 0.542 ms [37]. The dephasing time for AFC can reach $T_2 = 300 \pm 30 \mu\text{s}$ experimentally [38]

In particular, we consider a Stark-modulated AFC memory with an optical cavity [34] with the following considerations: We use d^2 AFC memories as needed for the QEC protocol. We also set the finesse of the comb $F_{\text{AFC}} = 40$, which relates with the memory retrieval probability η_{cav} as [34]:

$$\eta_{\text{cav}} = \frac{4(\bar{\alpha}l)^2 e^{-2\bar{\alpha}l} (1 - R_1)^2 R_2 e^{-t^2 \bar{\epsilon}^2}}{(1 - \sqrt{R_1 R_2} e^{-\bar{\alpha}l})^4}, \tag{10}$$

where t is the storage time of the photon, $\bar{\alpha} = \frac{\alpha}{F_{\text{AFC}}} \sqrt{\frac{\pi}{4\ln(2)}}$ is the effective absorption of the comb, α is the absorption coefficient of the comb peaks and l is the crystal length. $R_1 = 0.96$ and $R_2 = 0.99$ are the mirror reflectivities and $\bar{\epsilon} = \frac{2\pi\epsilon}{\sqrt{8\ln(2)}}$ is related to the comb FWHM ϵ . In our simulation, we used $\alpha l = 1$, with ϵ of 3 kHz and negligible inter-cavity loss. Experimentally, $F_{\text{AFC}} = 5.8$ achieved storage-retrieval efficiencies of $55 \pm 5\%$ [39] and 62% [32] for cavity-coupled AFCs. We expect our chosen parameters to be achievable for AFC with persistent holes and ϵ in the kHz range [34]. Our simulation did not consider the atomic dephasing dependence on comb finesse changes [40]. We assumed a 100% intrinsic efficiency to convert from kHz to telecom frequency, which may be achievable for single photons [41].

VI. RESULTS

Using Stim [42], we simulated the performance of both protocols for planar and rotated surface codes with $d = 3$ and $d = 5$, as well as Bacon-Shor codes, under both the standard (Section V-A) and robust noise models (Section V-B). The simulations were conducted using the Monte Carlo method with 10^8 events for the standard noise model and 10^5 events for the robust noise model. To decode X, Y , and Z errors, we employed a minimum-weight perfect matching algorithm implemented via the sparse blossom method, as detailed in [43].

A. Standard noise model

1) *Logical error rate*: Under the standard noise model, we examined in Fig.4 how physical error rates after each operation affect logical error rates over a single QEC iteration for logical Bell pairs in quantum memory. We observe pseudo-thresholds where physical error rates above $p_{\text{err}} = (5.5 \pm 0.2) \times 10^{-4}$ for $S[[18, 2, 3]]$, $p_{\text{err}} = (9.0 \pm 0.3) \times 10^{-4}$ for rotated $S[[18, 2, 3]]$, and $p_{\text{err}} = (1.5 \pm 0.2) \times 10^{-3}$ for the

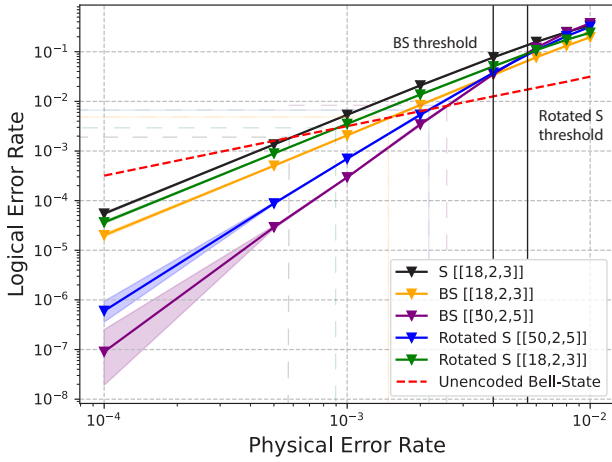


Fig. 4. One iteration of quantum error correction (QEC) for logical Bell pairs stored in the quantum memory is analyzed using the standard noise model outlined in Section V-A. The thresholds at which increasing the code distance (from $d = 3$ to $d = 5$) leads to a higher logical error rate are determined for both the *BS* and rotated *S* codes. Furthermore, the pseudo-thresholds are identified, indicating the noise levels at which QEC becomes beneficial by comparing the logical error rate of the codes to that of the unencoded Bell state.

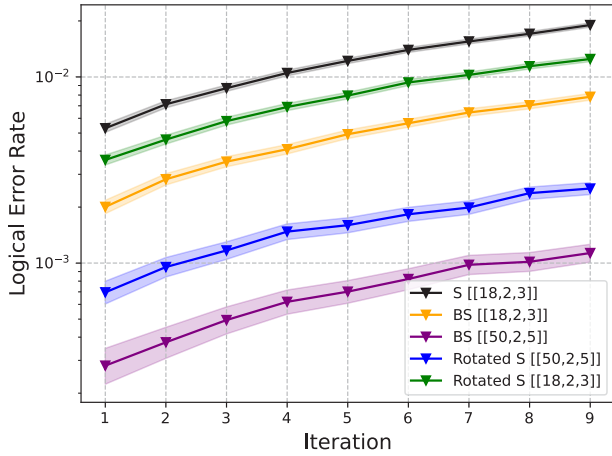


Fig. 5. 10 QEC iteration cycles of the logical Bell pairs while in a quantum memory using the standard noise model for $p_{\text{err}} = 10^{-3}$.

BS[[18, 2, 3]] codes show no advantage over unencoded Bell states. This extends the results of [9], where pseudo-thresholds of $p_{\text{err}} = 9.0 \times 10^{-3}$ for Bacon-Shor and $p_{\text{err}} = 1.5 \times 10^{-3}$ for surface codes were obtained without lattice surgery. Notice that compared to [9] our standard model considers depolarization for idle gates. These results apply to both protocols, as the standard noise model does not introduce significant differences between them.

In Fig. 5, we additionally studied the overall performance of the codes for $p_{\text{err}} = 10^{-3}$, where *BS* code outperformed both surface codes for 9 QEC syndrome extractions in the quantum memory, reaching for $d = 3$ a logical error of $p_L = (7.8 \pm 0.3) \times 10^{-3}$. Despite the standard noise model's usefulness for evaluating per gate operation errors, it does not account for photon loss during transportation and storage, and incorrect

photon detection, requiring a more robust evaluation of code viability.

2) *Code scalability*: To assess the scalability of the protocol in relation to code performance, we identified the threshold under a specific error model in which increasing the code distance results in a deterioration of the logical error rate. This was achieved by comparing the logical error rates of codes with distances $d = 3$ and $d = 5$ as a function of p_{err} .

For the standard noise model described in Section V-A, the thresholds were identified in Fig. 4 as $p_{\text{err}} = (3.9 \pm 0.1) \times 10^{-3}$ for *BS* codes and $p_{\text{err}} = (5.8 \pm 0.2) \times 10^{-3}$ for rotated *S* codes.

B. Robust noise model

1) *Logical error rate*: Using the error model from Table I, we calculate the time budget in Table II for each protocol and various QEC codes to perform one QEC iteration cycle ($t_{\text{QEC}} = t_{\text{cycle}}$) for the logical Bell states in the quantum memory at $D = 1$ km.

TABLE II
TIME BUDGET FOR ONE QEC CYCLE AT THE QUANTUM MEMORY FOR $D = 1$ km.

QEC code	t_{cycle}	t_{merge}	t_{travel}	t_{total}	Units
Protocol 1: <i>S</i> [[18, 2, 3]]	3.47	13.87	4.80	26.83	μs
Protocol 1: rotated <i>S</i> [[18, 2, 3]]	3.47	13.87	4.80	26.83	μs
Protocol 1: <i>BS</i> [[18, 2, 3]]	9.37	37.47	4.80	62.23	μs
Protocol 2: <i>S</i> [[18, 2, 3]]	3.47	13.87	14.41	36.43	μs
Protocol 2: rotated <i>S</i> [[18, 2, 3]]	3.47	13.87	14.41	36.43	μs
Protocol 2: <i>BS</i> [[18, 2, 3]]	9.37	37.47	14.41	71.83	μs

For both protocols, we created a scheduler to monitor the availability of quantum memories and logical Bell state generation hardware. We adopt an optimal approach, keeping Charlie and the nodes synchronized through continuous classical communication. In Fig. 8, for 10^5 events per iteration, we simulated all code and protocol combinations, including the unencoded Bell state, analyzing simulation parameters T_1 and T_2 and the overall error rate p_{err} for a distance of $D = 1$ km.

Instead of comparing codes based on syndrome measurements, we evaluate them in terms of storage time. This approach simplifies comparison due to differences in operational complexity among codes, as discussed in Appendix X-B. Because of the time requirements for *H*, *CX*, and measurement operations, a single QEC cycle of the Bacon-Shor code allows up to three syndrome extractions within surface codes in the same period of time.

In Fig. 8, we estimate the pseudo-threshold at which QEC becomes more advantageous than using the unencoded Bell state. For error rates below $0.1p_{\text{err}_H}$, $0.1p_{\text{err}_{CX}}$, and $0.1p_{\text{err}_M}$, both rotated and planar surface codes are viable. A similar trend is observed for Bacon-Shor codes with multiple iteration cycles, although they suffer from initialization complexity when creating logical Bell states. This result is crucial as it defines the minimal hardware requirements under the stated assumptions for which QEC is viable in superconducting systems specifically when used in quantum memories (AFC memories) for logical Bell state protocols.

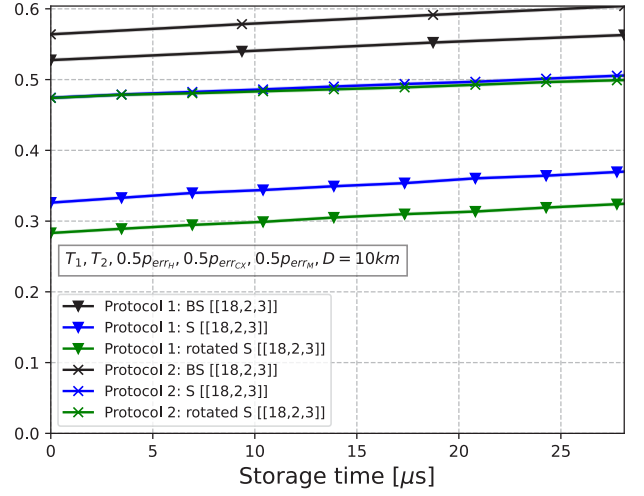
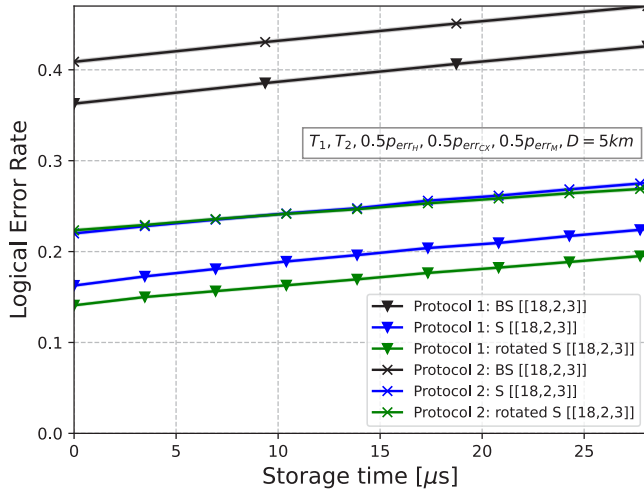


Fig. 6. Comparison of the logical error rate [10] of protocols 1 and 2 for code distance $d = 3$ in terms of the quantum memory storage time for T_1 , T_2 and $0.5p_{\text{err}_H}$, $0.5p_{\text{err}_{CX}}$, $0.5p_{\text{err}_M}$ for distances (D) of 5 km and 10 km between the nodes and Charlie.

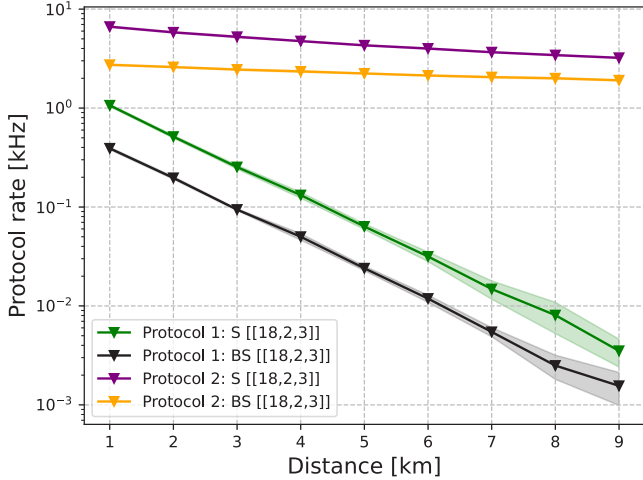


Fig. 7. Protocol rate in terms of operational distance between Charlie and the nodes for one QEC cycle of the logical Bell pair in the quantum memory.

Additionally, we examined performance at various distances, as shown in Fig. 6 for $D = 5$ km and 10 km. We find that the logical error rate rises in both protocols, to the point where the protocol 2, using a surface code, converges with the protocol 1, which uses the Bacon-Shor code, as shown in Fig. 6 (right).

2) *Code scalability*: For the noise model defined in Section V-B we have calculated the family code threshold by evaluating at which ratio of gate errors p_{err_H} , $p_{\text{err}_{CX}}$, p_{err_M} increasing the code distance no longer increases the logical error rate. For $2T_1$ and $2T_2$ in rotated S we found this threshold at a ratio of 0.58 ± 0.01 . For BS codes, the high error per QEC cycle, as explained in Appendix X-B, results in a threshold that is two orders of magnitude lower compared to surface codes.

3) *Protocol rate*: In Fig. 7, we calculated the success rate of each protocol based on 10^4 sequential state generations, varying the distance between Charlie and the nodes (Alice and Bob) from 1 to 9 km. We assume that only one logical Bell pair is created at a time, and no parallel merging or splitting operations occur, which constrains processing time. The scheduler tracks the local time of each logical Bell pair, and the protocol rate depends not on the fidelity of the logical Bell pairs but on successful detection at the nodes, meaning no dark counts or photon loss within the detector's capture window, as well as successful recovery of data qubits from quantum memory. The standard deviation for each point is derived from 10 repetitions, each using a different seed for the 10^4 Bell state generations. Given their similar time complexities, the rotated and planar surface codes are grouped.

As shown in Fig. 7, protocol 2 demonstrates a clear advantage in terms of success rate R_{success} , achieving values in the range $R_{\text{success}} \in [6.64 \pm 0.12, 3.22 \pm 0.04]$ kHz for $S[[18, 2, 3]]$ and $R_{\text{success}} \in [2.74 \pm 0.05, 1.91 \pm 0.03]$ kHz for $BS[[18, 2, 3]]$, for distances between 1 km and 9 km between the nodes and a trusted party. This advantage is mainly due to the high source frequency f_{source} for auxiliary Bell pair generation during node merging operations. By contrast, the protocol 1 requires aborting if any data qubits are lost, leading to significantly lower rates at longer distances.

VII. CONCLUSIONS

This study aims to bridge the existing research gap by conducting detailed simulations to generate logical Bell pairs using Quantum Error Correction (QEC) techniques. QEC is critical in second and third-generation quantum repeaters for maintaining state integrity during distillation and entanglement swapping. For the first time, we explore the feasibility of performing and storing logical Bell states through two innovative logical heralded entanglement protocols: one local and one

non-local. Our comprehensive analysis delves into the physical parameters, minimal requirements, and challenges associated with generating and storing logical Bell pairs within cavity-enhanced Atomic Frequency Comb (AFC) memories. We assess rotated and planar surface codes alongside Bacon-Shor codes, which can be implemented with low code distances considering existing hardware.

Two noise models are considered for logical heralded entanglement: a standard noise model (Section V-A) and a more realistic one (Section V-B). We identified the pseudo-thresholds where exceeding the physical error offers no advantage over unencoded Bell states in either protocol. By comparing $d = 3$ and $d = 5$ codes we have also established thresholds beyond which increasing code distances degrade logical error rates (p_L). To evaluate protocol feasibility, we compared their rates. The non-local protocol demonstrated a clear advantage, with $S[[18, 2, 3]]$ achieving success rates of $R_{\text{success}} \in [6.64 \pm 0.12, 3.22 \pm 0.04]$ kHz across node-to-Charlie distances of 1 km to 9 km.

We reevaluated the pseudo-thresholds in terms of gate error rates p_{err_H} , $p_{\text{err}_{CX}}$, and p_{err_M} , with parameters provided in Table I. For a node-to-Charlie distance of $D = 1$ km, achieving an advantage over an unencoded Bell state heralded protocol requires reducing gate error rates by an order of magnitude ($0.1p_{\text{err}_H}$, $0.1p_{\text{err}_{CX}}$, and $0.1p_{\text{err}_M}$). These results underscore the significant hardware improvements needed to implement logical Bell state protocols in quantum memories.

Future research could investigate leveraging unused logical qubits in quantum error-correcting codes to enhance redundancy and improve the fidelity of logical states. For higher number of data qubits, comparing BB codes to S and B codes might further highlight their scalability advantages and challenges of implementing them in a quantum network scenario. However, this approach would first require addressing the challenges posed by cyclic boundary conditions, which could be mitigated through equivalent and additional operations implemented in the hardware. Addressing cyclic boundary conditions, potentially through hardware modifications like using Rydberg atoms [44], remains an important step toward the practical implementation of these codes in quantum repeater protocols.

VIII. CODE AVAILABILITY

All codes responsible for the results in this article can be found at: <https://github.com/terrordayvg/Logical-Bell-States>.

IX. ACKNOWLEDGMENTS

The VG and JN acknowledge the financial support by the Federal Ministry of Education and Research of Germany in the program of “Souverän. Digital. Vernetzt”. Joint project 6G-life, project identification numbers: 16KISK002 and 16KISK263. Furthermore, VG and JN acknowledge the financial support under projects 16KISQ039, 16KISQ077 and 16KISQ168 and by the DFG via project NO 1129/2-1. VG also extends gratitude to Pol Julià Farré for reviewing the earlier versions of the article.

REFERENCES

- [1] S. Wehner, D. Elkouss, and R. Hanson, “Quantum internet: A vision for the road ahead,” *Science*, vol. 362, no. 6412, p. eaam9288, 2018. [Online]. Available: <https://www.science.org/doi/abs/10.1126/science.aam9288>
- [2] S. Muralidharan, L. Li, J. Kim, N. Lütkenhaus, M. D. Lukin, and L. Jiang, “Optimal architectures for long distance quantum communication,” *Scientific Reports*, vol. 6, 2015. [Online]. Available: <https://api.semanticscholar.org/CorpusID:14597684>
- [3] K. Azuma, S. E. Economou, D. Elkouss, P. Hilaire, L. Jiang, H.-K. Lo, and I. Tzitrin, “Quantum repeaters: From quantum networks to the quantum internet,” *Rev. Mod. Phys.*, vol. 95, p. 045006, Dec 2023. [Online]. Available: <https://link.aps.org/doi/10.1103/RevModPhys.95.045006>
- [4] K. Azuma, H. Takeda, M. Koashi, and N. Imoto, “Quantum repeaters and computation by a single module: Remote nondestructive parity measurement,” *Physical Review A*, vol. 85, no. 6, Jun. 2012. [Online]. Available: <http://dx.doi.org/10.1103/PhysRevA.85.062309>
- [5] X. Liu, J. Hu, Z.-F. Li, X. Li, P.-Y. Li, P.-J. Liang, Z.-Q. Zhou, C.-F. Li, and G.-C. Guo, “Heralded entanglement distribution between two absorptive quantum memories,” *Nature*, vol. 594, no. 7861, pp. 41–45, Jun. 2021.
- [6] D. Lago-Rivera, S. Grandi, J. V. Rakonjac, A. Seri, and H. de Ridmaten, “Telecom-heralded entanglement between multimode solid-state quantum memories,” *Nature*, vol. 594, no. 7861, p. 37–40, Jun. 2021. [Online]. Available: <http://dx.doi.org/10.1038/s41586-021-03481-8>
- [7] M. Pompili, S. L. N. Hermans, S. Baier, H. K. C. Beukers, P. C. Humphreys, R. N. Schouten, R. F. L. Vermeulen, M. J. Tiggeleman, L. dos Santos Martins, B. Dirkse, S. Wehner, and R. Hanson, “Realization of a multinode quantum network of remote solid-state qubits,” *Science*, vol. 372, no. 6539, p. 259–264, Apr. 2021. [Online]. Available: <http://dx.doi.org/10.1126/science.abg1919>
- [8] V. Krutyanskiy, M. Galli, V. Krcmarsky, S. Baier, D. Fioretto, Y. Pu, A. Mazloom, P. Sekatski, M. Canteri, M. Teller, J. Schupp, J. Bate, M. Meraner, N. Sangouard, B. Lanyon, and T. Northup, “Entanglement of trapped-ion qubits separated by 230 meters,” *Physical Review Letters*, vol. 130, no. 5, Feb. 2023. [Online]. Available: <http://dx.doi.org/10.1103/PhysRevLett.130.050803>
- [9] M. Li, D. Miller, and K. R. Brown, “Direct measurement of bacon-shor code stabilizers,” *Phys. Rev. A*, vol. 98, p. 050301, Nov 2018. [Online]. Available: <https://link.aps.org/doi/10.1103/PhysRevA.98.050301>
- [10] A. Katabarwa and M. R. Geller, “Logical error rate in the pauli twirling approximation,” *Scientific Reports*, vol. 5, no. 1, p. 14670, Sep 2015. [Online]. Available: <https://doi.org/10.1038/srep14670>
- [11] D. Horsman, A. G. Fowler, S. Devitt, and R. V. Meter, “Surface code quantum computing by lattice surgery,” *New Journal of Physics*, vol. 14, no. 12, p. 123011, Dec. 2012. [Online]. Available: <http://dx.doi.org/10.1088/1367-2630/14/12/123011>
- [12] A. Cowtan and S. Burton, “CSS code surgery as a universal construction,” *Quantum*, vol. 8, p. 1344, May 2024. [Online]. Available: <https://doi.org/10.22331/q-2024-05-14-1344>
- [13] K. M. Svore, A. W. Cross, I. L. Chuang, and A. V. Aho, “A flow-map model for analyzing pseudothresholds in fault-tolerant quantum computing,” 2006. [Online]. Available: <https://arxiv.org/abs/quant-ph/0508176>
- [14] Q. Xu, J. P. Bonilla Ataides, C. A. Pattison, N. Raveendran, D. Bluvstein, J. Wurtz, B. Vasić, M. D. Lukin, L. Jiang, and H. Zhou, “Constant-overhead fault-tolerant quantum computation with reconfigurable atom arrays,” *Nature Physics*, vol. 20, no. 7, pp. 1084–1090, Jul 2024. [Online]. Available: <https://doi.org/10.1038/s41567-024-02479-z>
- [15] L. Z. Cohen, I. H. Kim, S. D. Bartlett, and B. J. Brown, “Low-overhead fault-tolerant quantum computing using long-range connectivity,” *Science Advances*, vol. 8, no. 20, May 2022. [Online]. Available: <http://dx.doi.org/10.1126/sciadv.abn1717>
- [16] N. P. Breuckmann and J. N. Eberhardt, “Balanced product quantum codes,” *IEEE Transactions on Information Theory*, vol. 67, no. 10, p. 6653–6674, Oct. 2021. [Online]. Available: <http://dx.doi.org/10.1109/TIT.2021.3097347>
- [17] S. Bravyi, A. W. Cross, J. M. Gambetta, D. Maslov, P. Rall, and T. J. Yoder, “High-threshold and low-overhead fault-tolerant quantum memory,” *Nature*, vol. 627, no. 8005, pp. 778–782, Mar 2024. [Online]. Available: <https://doi.org/10.1038/s41586-024-07107-7>

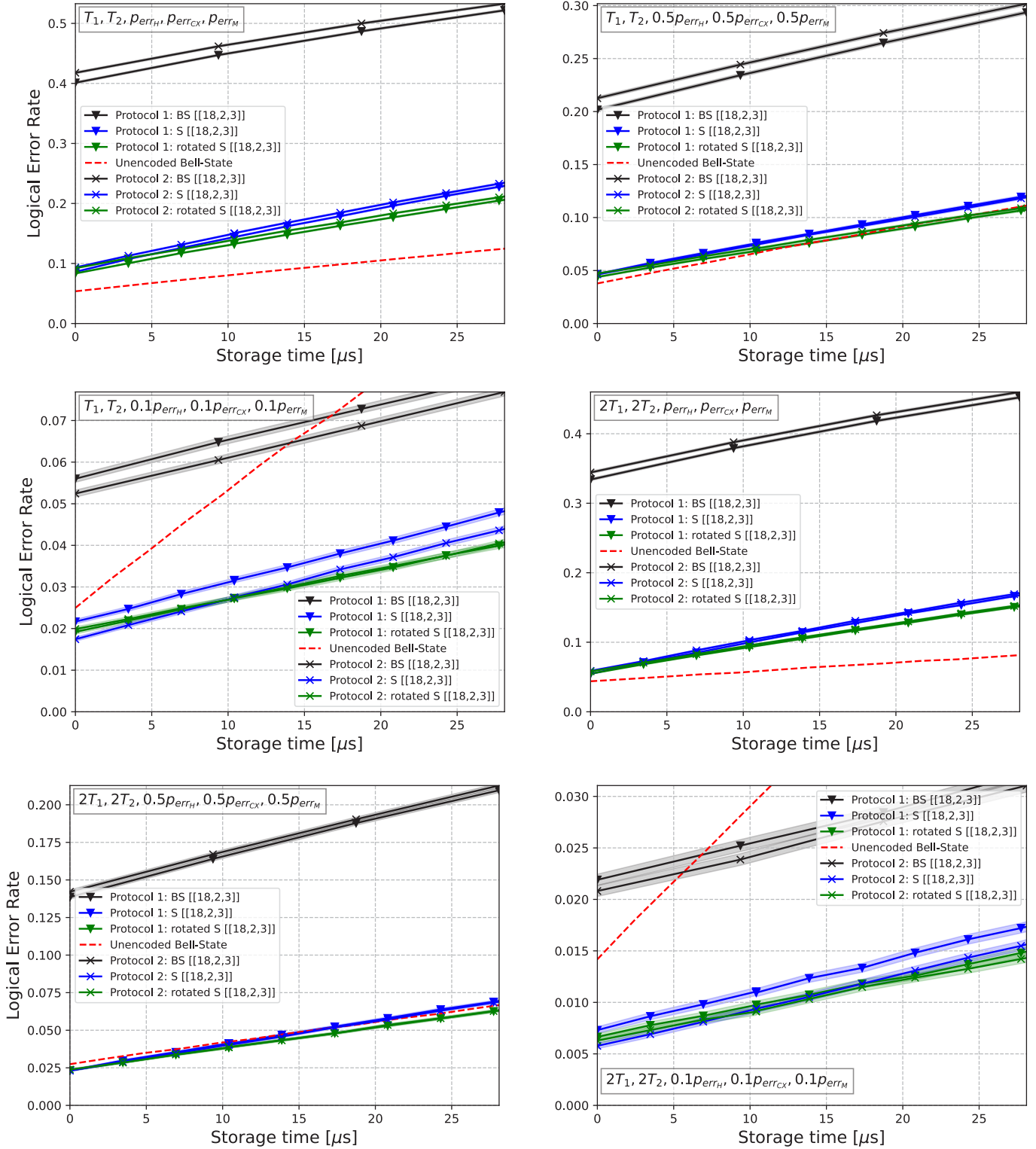


Fig. 8. Storage time dependency for surface and Bacon-Shor codes of code distance $d = 3$ with decoherence T_1 and dephasing times T_2 with overall gate error $p_{\text{err}_H}, p_{\text{err}_{CX}}, p_{\text{err}_M}$ according to the Table.I. To find a viable threshold to perform QEC for each code we have varied these parameters accordingly.

- [18] B. Hetényi and J. R. Wootton, "Creating entangled logical qubits in the heavy-hex lattice with topological codes," 2024. [Online]. Available: <https://arxiv.org/abs/2404.15989>
- [19] D. Litinski, "A game of surface codes: Large-scale quantum computing with lattice surgery," *Quantum*, vol. 3, p. 128, Mar. 2019. [Online]. Available: <http://dx.doi.org/10.22331/q-2019-03-05-128>
- [20] A. Bocharov, M. Roetteler, and K. M. Svore, "Efficient synthesis of universal repeat-until-success quantum circuits," *Phys. Rev. Lett.*, vol. 114, p. 080502, Feb 2015. [Online]. Available: <https://link.aps.org/doi/10.1103/PhysRevLett.114.080502>
- [21] D. B. Tan, M. Y. Niu, and C. Gidney, "A sat scalpel for lattice surgery: Representation and synthesis of subroutines for surface-code fault-tolerant quantum computing," in *2024 ACM/IEEE 51st Annual International Symposium on Computer Architecture (ISCA)*. IEEE, Jun. 2024, p. 325–339. [Online]. Available: <http://dx.doi.org/10.1109/ISCA59077.2024.00032>
- [22] N. de Beaudrap and D. Horsman, "The ZX calculus is a language for surface code lattice surgery," *Quantum*, vol. 4, p. 218, Jan. 2020. [Online]. Available: <https://doi.org/10.22331/q-2020-01-09-218>
- [23] C. Gidney and D. Bacon, "Less bacon more threshold," 2023. [Online]. Available: <https://arxiv.org/abs/2305.12046>
- [24] A. Erhard, H. Poulsen Nautrup, M. Meth, L. Postler, R. Stricker, M. Stadler, V. Negnevitsky, M. Ringbauer, P. Schindler, H. J. Briegel, R. Blatt, N. Friis, and T. Monz, "Entangling logical qubits with lattice surgery," *Nature*, vol. 589, no. 7841, pp. 220–224, Jan 2021. [Online]. Available: <https://doi.org/10.1038/s41586-020-03079-6>
- [25] W. J. Munro, K. Azuma, K. Tamaki, and K. Nemoto, "Inside quantum repeaters," *IEEE Journal of Selected Topics in Quantum Electronics*, vol. 21, no. 3, pp. 78–90, 2015.
- [26] Y. Tomita and K. M. Svore, "Low-distance surface codes under realistic quantum noise," *Phys. Rev. A*, vol. 90, p. 062320, Dec 2014. [Online]. Available: <https://link.aps.org/doi/10.1103/PhysRevA.90.062320>
- [27] Z. Cai and S. C. Benjamin, "Constructing smaller pauli twirling sets for arbitrary error channels," *Scientific Reports*, vol. 9, no. 1, p. 11281, Aug 2019. [Online]. Available: <https://doi.org/10.1038/s41598-019-46722-7>
- [28] J. Ghosh, A. G. Fowler, and M. R. Geller, "Surface code with decoherence: An analysis of three superconducting architectures," *Phys. Rev. A*, vol. 86, p. 062318, Dec 2012. [Online]. Available: <https://link.aps.org/doi/10.1103/PhysRevA.86.062318>
- [29] X. Liu, J. Hu, Z.-F. Li, X. Li, P.-Y. Li, P.-J. Liang, Z.-Q. Zhou, C.-F. Li, and G.-C. Guo, "Heralded entanglement distribution between two absorptive quantum memories," *Nature*, vol. 594, no. 7861, pp. 41–45, Jun 2021. [Online]. Available: <https://doi.org/10.1038/s41586-021-03505-3>
- [30] M. Rančić, M. P. Hedges, R. L. Ahlefeldt, and M. J. Sellars, "Coherence time of over a second in a telecom-compatible quantum memory storage material," *Nature Physics*, vol. 14, no. 1, pp. 50–54, Jan 2018. [Online]. Available: <https://doi.org/10.1038/nphys4254>
- [31] T. Coopmans, R. Knegjens, A. Dahlberg, D. Maier, L. Nijsten, J. de Oliveira Filho, M. Papendrecht, J. Rabbie, F. Rozpkedek, M. Skrzypczyk, L. Wubben, W. de Jong, D. Podareanu, A. Torres-Knoop, D. Elkouss, and S. Wehner, "Netsquid, a network simulator for quantum information using discrete events," *Communications Physics*, vol. 4, no. 1, p. 164, Jul 2021. [Online]. Available: <https://doi.org/10.1038/s42005-021-00647-8>
- [32] S. Duranti, S. Wengerowsky, L. Feldmann, A. Seri, B. Casabone, and H. de Riedmatten, "Efficient cavity-assisted storage of photonic qubits in a solid-state quantum memory," 2023.
- [33] Y. Ma, Y.-Z. Ma, Z.-Q. Zhou, C.-F. Li, and G.-C. Guo, "One-hour coherent optical storage in an atomic frequency comb memory," *Nature Communications*, vol. 12, no. 1, p. 2381, Apr 2021. [Online]. Available: <https://doi.org/10.1038/s41467-021-22706-y>
- [34] S. P. Horvath, M. K. Alqedra, A. Kinoshita, A. Walther, J. M. Dahlström, S. Kröll, and L. Rippe, "Noise-free on-demand atomic frequency comb quantum memory," *Phys. Rev. Res.*, vol. 3, p. 023099, May 2021. [Online]. Available: <https://link.aps.org/doi/10.1103/PhysRevResearch.3.023099>
- [35] A. Seri, D. Lago-Rivera, A. Lenhard, G. Corrielli, R. Osellame, M. Mazzer, and H. de Riedmatten, "Quantum storage of frequency-multiplexed heralded single photons," *Phys. Rev. Lett.*, vol. 123, p. 080502, Aug 2019. [Online]. Available: <https://link.aps.org/doi/10.1103/PhysRevLett.123.080502>
- [36] M. Bonarota, J.-L. L. Gouët, and T. Chanelière, "Highly multimode storage in a crystal," *New Journal of Physics*, vol. 13, no. 1, p. 013013, Jan 2011. [Online]. Available: <https://dx.doi.org/10.1088/1367-2630/13/1/013013>
- [37] P. Jobez, N. Timoney, C. Laplane, J. Etesse, A. Ferrier, P. Goldner, N. Gisin, and M. Afzelius, "Towards highly multimode optical quantum memory for quantum repeaters," *Phys. Rev. A*, vol. 93, p. 032327, Mar 2016. [Online]. Available: <https://link.aps.org/doi/10.1103/PhysRevA.93.032327>
- [38] A. Ortu, J. V. Rakonjac, A. Holzäpfel, A. Seri, S. Grandi, M. Mazzer, H. de Riedmatten, and M. Afzelius, "Multimode capacity of atomic-frequency comb quantum memories," *Quantum Science and Technology*, vol. 7, no. 3, p. 035024, Jun. 2022. [Online]. Available: <http://dx.doi.org/10.1088/2058-9565/ac73b0>
- [39] M. Sabooni, Q. Li, S. Kröll, and L. Rippe, "Efficient quantum memory using a weakly absorbing sample," *Phys. Rev. Lett.*, vol. 110, p. 133604, Mar 2013. [Online]. Available: <https://link.aps.org/doi/10.1103/PhysRevLett.110.133604>
- [40] M. Afzelius and C. Simon, "Impedance-matched cavity quantum memory," *Phys. Rev. A*, vol. 82, p. 022310, Aug 2010. [Online]. Available: <https://link.aps.org/doi/10.1103/PhysRevA.82.022310>
- [41] L. Ma, O. Slattery, and X. Tang, "Single photon frequency up-conversion and its applications," *Physics Reports*, vol. 521, no. 2, pp. 69–94, 2012, single photon frequency up-conversion and its applications. [Online]. Available: <https://www.sciencedirect.com/science/article/pii/S0370157312002384>
- [42] C. Gidney, "Stim: a fast stabilizer circuit simulator," *Quantum*, vol. 5, p. 497, Jul. 2021. [Online]. Available: <https://doi.org/10.22331/q-2021-07-06-497>
- [43] O. Higgott and C. Gidney, "Sparse blossom: correcting a million errors per core second with minimum-weight matching," 2023. [Online]. Available: <https://arxiv.org/abs/2303.15933>
- [44] C. Poole, T. M. Graham, M. A. Perlin, M. Otten, and M. Saffman, "Architecture for fast implementation of qldpc codes with optimized rydberg gates," 2024. [Online]. Available: <https://arxiv.org/abs/2404.18809>
- [45] A. deMarti iOlius, P. Fuentes, R. Orús, P. M. Crespo, and J. Etxezarreta Martinez, "Decoding algorithms for surface codes," *Quantum*, vol. 8, p. 1498, Oct. 2024. [Online]. Available: <https://doi.org/10.22331/q-2024-10-10-1498>
- [46] R. Acharya, I. Aleiner, R. Allen, T. I. Andersen, M. Ansmann, F. Arute, K. Arya, A. Asfaw, J. Atalaya, R. Babush, D. Bacon, J. C. Bardin, J. Basso, A. Bengtsson, S. Boixo, G. Bortoli, A. Bourassa, J. Bovaird, L. Brill, M. Broughton, B. B. Buckley, D. A. Buell, T. Burger, B. Burkett, N. Bushnell, Y. Chen, Z. Chen, B. Chiaro, J. Cogán, R. Collins, P. Conner, W. Courtney, A. L. Crook, B. Curtin, D. M. Debroy, A. Del Toro Barba, S. Demura, A. Dunsworth, D. Eppens, C. Erickson, L. Faoro, E. Farhi, R. Fatemi, L. Flores Burgos, E. Forati, A. G. Fowler, B. Foxen, W. Giang, C. Gidney, D. Gilboa, M. Giustina, A. Grajales Dau, J. A. Gross, S. Habegger, M. C. Hamilton, M. P. Harrigan, S. D. Harrington, O. Higgott, J. Hilton, M. Hoffmann, S. Hong, T. Huang, A. Huff, W. J. Huggins, L. B. Ioffe, S. V. Isakov, J. Iveland, E. Jeffrey, Z. Jiang, C. Jones, P. Juhas, D. Kafri, K. Kechedzhi, J. Kelly, T. Khattar, M. Khezri, M. Kieferová, S. Kim, A. Kitaev, P. V. Klimov, A. R. Klots, A. N. Korotkov, F. Kostritsa, J. M. Kreikebaum, D. Landhuis, P. Laptev, K.-M. Lau, L. Laws, J. Lee, K. Lee, B. J. Lester, A. Lill, W. Liu, A. Locharla, E. Lucero, F. D. Malone, J. Marshall, O. Martin, J. R. McClean, T. McCourt, M. McEwen, A. Megrant, B. Meurer Costa, X. Mi, K. C. Miao, M. Mohseni, S. Montazeri, A. Morvan, E. Mount, W. Mruczkiewicz, O. Naaman, M. Neeley, C. Neill, A. Nersisyan, H. Neven, M. Newman, J. H. Ng, A. Nguyen, M. Nguyen, M. Y. Niu, T. E. O'Brien, A. Opremcak, J. Platt, A. Petukhov, R. Potter, L. P. Pryadko, C. Quintana, P. Roushan, N. C. Rubin, N. Saei, D. Sank, K. Sankaragomathi, K. J. Satzinger, H. F. Schurkus, C. Schuster, M. J. Shearn, A. Shorter, V. Shvarts, J. Skrzynski, V. Smelyanskiy, W. C. Smith, G. Sterling, D. Strain, M. Szalay, A. Torres, G. Vidal, B. Villalonga, C. Vollgraf Heidweiller, T. White, C. Xing, Z. J. Yao, P. Yeh, J. Yoo, G. Young, A. Zalcman, Y. Zhang, N. Zhu, and G. Q. Ai, "Suppressing quantum errors by scaling a surface code logical qubit," *Nature*, vol. 614, no. 7949, pp. 676–681, Feb 2023. [Online]. Available: <https://doi.org/10.1038/s41586-022-05434-1>
- [47] P. Aliferis and A. W. Cross, "Subsystem fault tolerance with the Bacon-Shor code," *Phys. Rev. Lett.*, vol. 98, p. 220502, May 2007. [Online]. Available: <https://link.aps.org/doi/10.1103/PhysRevLett.98.220502>

- [48] L. Egan, D. M. Debroy, C. Noel, A. Risinger, D. Zhu, D. Biswas, M. Newman, M. Li, K. R. Brown, M. Cetina, and C. Monroe, "Fault-tolerant operation of a quantum error-correction code," 2021. [Online]. Available: <https://arxiv.org/abs/2009.11482>
- [49] M. Gutiérrez, M. Müller, and A. Bermúdez, "Transversality and lattice surgery: Exploring realistic routes toward coupled logical qubits with trapped-ion quantum processors," *Phys. Rev. A*, vol. 99, p. 022330, Feb 2019. [Online]. Available: <https://link.aps.org/doi/10.1103/PhysRevA.99.022330>
- [50] R. Raussendorf, J. Harrington, and K. Goyal, "Topological fault-tolerance in cluster state quantum computation," *New Journal of Physics*, vol. 9, no. 6, p. 199–199, Jun. 2007. [Online]. Available: <http://dx.doi.org/10.1088/1367-2630/9/6/199>
- [51] A. G. Fowler, M. Mariantoni, J. M. Martinis, and A. N. Cleland, "Surface codes: Towards practical large-scale quantum computation," *Physical Review A*, vol. 86, no. 3, Sep. 2012. [Online]. Available: <http://dx.doi.org/10.1103/PhysRevA.86.032324>
- [52] D. Gottesman and I. L. Chuang, "Demonstrating the viability of universal quantum computation using teleportation and single-qubit operations," *Nature*, vol. 402, no. 6760, pp. 390–393, Nov 1999. [Online]. Available: <https://doi.org/10.1038/46503>
- [53] S. Bravyi and A. Kitaev, "Universal quantum computation with ideal clifford gates and noisy ancillas," *Phys. Rev. A*, vol. 71, p. 022316, Feb 2005. [Online]. Available: <https://link.aps.org/doi/10.1103/PhysRevA.71.022316>

X. APPENDIX

A. Indepth view of QEC codes

1) *Surface codes*: Surface codes encode d^2 data qubits into a single logical qubit, requiring $d^2 - 1$ syndrome qubits to measure X and Z syndromes per error correction cycle (Fig. 1), where d is the code distance which corresponds to the maximum length of error chains that can be reliably detected and corrected by the decoding algorithm.

Logical operations X_L and Z_L are implemented as products of Pauli operators, connecting opposite boundaries of the code. During each quantum error correction cycle, syndromes are measured for adjacent data qubits in a specific sequence with arrows, alternating between X and Z stabilizer measurements as (Fig. 1). When an error occurs, the corresponding measurement outcome flips its sign. If fewer than $(d - 1)/2$ errors occur, each measured syndrome can be associated with a correction operation. A decoder [45] then estimates the error and applies a correction, restoring the system to the stabilizer $+1$ state without introducing a logical error.

Surface codes offer a high threshold of 1%, rapid decoding algorithms, and compatibility with two-dimensional lattice architectures in quantum processors. Experimental studies, such as Acharya et al. (2023) [46], demonstrate their effectiveness, showing better logical error performance for distance-5 surface codes compared to averaged distance-3 surface codes in terms of logical error probability and error per cycle.

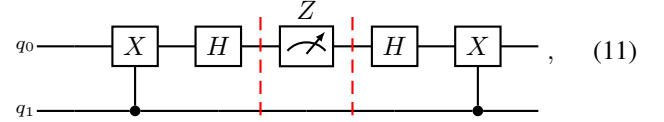
2) *Bacon-Shor codes*: Bacon-Shor codes [47] work similarly as surface codes, however they are built on a $L \times L$ planar lattice where $2(L - 1)$ weight- $2L$ stabilizers are inferred from measurements of $(L - 1)^2$ weight-2 gauge operators built as two-qubit parity measurements as seen in [9]. Each horizontal and vertical connection between qubits corresponds to $X \otimes X$ and $Z \otimes Z$ measurements, respectively. At each quantum error correction cycle the total parity of all data qubits is measured in Z and X basis, corresponding to $Z_L = Z_1, \dots, Z_d$ and $X_L = X_1, \dots, X_d$.

Bacon-Shor codes enhance protection against noisy channels by encoding logical qubits with non-commuting gauge operators. They offer benefits in qubit requirements and processing times for small distances but lack scalability to very low error rates [23]. Experimental implementations are detailed in [48] and [9].

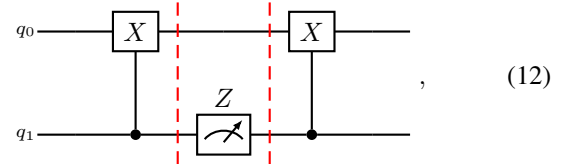
Most experimental QEC efforts focus on logical single qubits due to current hardware limitations, including noise levels and decoding complexities. Techniques for logical multi-qubit operations include transversality [49], braiding [50], [51], gate teleportation [52], magic state distillation [53], and lattice surgery [11], [22], with lattice surgery being preferred for its lower resource overhead.

B. Two-qubit X and Z basis parity measurement

To define the noise model for the two-qubit X or Z -basis parity measurement (M_{ZZ} and M_{XX} respectively) operations in the context of IBM Sherbrooke, we consider an equivalent decomposition into H , CX , and Z -basis measurement operations as no native M_{ZZ} and M_{XX} gates are available to the IBM processor. The decomposition for M_{XX} , which measures parity in the X -basis, can be expressed as follows (up to a global phase):



and the decomposition for the M_{ZZ} :



We consider half of the gate error and decoherence and dephasing noise of the idle gates before the measurement operation and the other half afterwards. This transpilation also implies an added gate and time complexity $t_{cycle} = 4t_M + 8t_{CX} + 8t_H$ compared to surface codes $t_{cycle} = 2t_H + 4t_{CX} + t_M$.